Preparation of Nanoscale Inorganic $CsPbI_xBr_{3-x}$ Perovskite Photosensitizers on the Surface of Mesoporous TiO_2 Film for Solid-State Sensitized Solar Cells

So-Min Yoo,[a,†] Seul-Yi Lee,[a,†] Gitae Kim, [a] Esteban Velilla Hernandez,[b,c] Iván Mora-Seró,[b] Seog Joon Yoon, [b,d] Taeho Shin, [a] Sel-Hi Lee,[e,f] Seok-Hoon Ahn,[f] Min-Kyoung Song, [g] Myoung Kim,[a,] and Hyo Joong Lee [a,e]**

Department of Chemistry, Jeonbuk National University, Jeonju, 561-756, South Korea (ROK),[a] Institute of Advanced Materials (INAM), University Jaume I, Avenida de Vicent Sos Baynat, s/n, 12071 Castelló de la Plana, Spain,[b] Centro de Investigación, Innovación y Desarrollo de Materiales-CIDEMAT, Universidad de Antioquia UdeA, Calle 70 No. 52-21, Medellín, Colombia,[c] Department of Chemistry, College of Natural Science, Yeungnam University, 280 Daehak-Ro, Gyeongsan, Gyeongbuk 38541, South Korea (ROK),[d] Department of Bioactive Material Sciences, Jeonbuk National University, Jeonju, 561-756, South Korea (ROK),[e] Institute of Advanced Composite Materials, Korea Institute of Science and Technology (KIST), Jeonbuk, 565-905, South Korea (ROK),[f] Center for University-Wide Research Facilities (CURF), Jeonbuk National University, Jeonju, 561-756, South Korea (ROK)[g]

*To whom correspondence should be addressed: myoung@jbnu.ac.kr (M. Kim), solarlee@jbnu.ac.kr (H. J. Lee)

S.-M. Yoo† and S.-Y. Lee† contributed equally.

Tel.:+82-63-270-3353, Fax: +82-63-270-3408.

ABSTRACT

Metal chalcogenide quantum dot (QD)-like all-inorganic nanoscale perovskite photosensitizers of $CsPbI_xBr_{3-x}$ were prepared on the surface of mesoscopic TiO_2 film by a direct two-step spin-coating of lead and cesium halide precursors for application into solid-state dye-sensitized solar cells (DSSCs), as confirmed by impedance frequency response analysis. A few nanometer-sized hemisphere-shaped dots of $CsPbI_xBr_{3-x}$ perovskites were deposited and distributed separately onto TiO_2, which were checked by scanning and transmission electron microscopic (SEM and TEM) techniques. The as-deposited $CsPbI_xBr_{3-x}$ perovskites were stable only in the case of including about 20% or more bromide in the composition of halides. When the bromide content increased in the ratio of halides of $CsPbI_xBr_{3-x}$, gradual decrease in lattice spacing and blue-shift of emission peaks were observed in X-ray diffraction (XRD) and photoluminescence (PL) measurements, respectively. These well-defined nano-particulate $CsPbI_xBr_{3-x}$ perovskites were incorporated into solid-state DSSCs and tested as a new type of photosensitizers. The initial power conversion efficiency (PCE) of ca. 1.0 ~ 3.5 % based on relatively thin mesoporous TiO_2 film (~1 μm) looks promising with many parameters remaining for possibly more optimization. The best result, 3.79 %, was obtained from $CsPbI_{2.2}Br_{0.80}$ 25 days after initial measurement. These $CsPbI_xBr_{3-x}$-sensitized cells displayed a stable record of PCE over ~2 month and no hysteresis behavior in current-voltage traces.

KEYWORDS: Nanoscale perovskites, photosensitizer, inorganic perovskites, two-step deposition, dye-sensitized solar cells, impedance frequency response.

1. Introduction

Recently, big progress has been made in the overall power conversion efficiency (PCE) of quantum dot (QD)-sensitized solar cells (SSCs) with polysulfide-based liquid electrolytes, approaching ~13% [1-4] which is almost the same as the best result of typical molecular dye-sensitized solar cells (DSSCs) using a redox couple in solution [5-7]. This advancement was possible mainly due to (1) a proper preparation of colloidal QDs with an ideal band gap of 1.3-1.5 eV [8,9], (2) finding an effective adsorption route for colloidal QDs on the surface of mesoporous metal oxide films [10,11], and (3) enhanced interfacial modifications to reduce recombination at the interfaces [12,13]. However, in terms of stability, these liquid-type QD SSCs have not shown a behavior of robust maintenance for a long time due to easy volatility, slow leakage, and the strong alkalinity (pH value > 10) of polysulfide liquid electrolytes. In the meantime, solid-state QD-sensitized solar cells have also been developed at a very slow pace, now attaining a broad range of PCE between 1.0 and 8.0 % depending on the cells investigated [14-18]. In the solid version, liquid electrolytes were replaced with solid hole-transporting materials (HTM) where organic monomers (spiro-OMeTAD) or polymers [poly 3-hexylthiophene (P3HT) or others] were generally adopted and filled inside relatively thin mesoporous metal oxide electrodes as typical examples of HTM. Thus far, the best results (5~8 %) were obtained in very few cases from chemical bath-deposited Sb_2S_3 [16,17] or attached colloidal PbS QDs [18] as sensitizer and a few polymers as HTM in a thinner than about 1 μm TiO_2 film. These less-efficient results are mainly attributed to a low short-circuit current (J_{sc}) due to the use of thinner mesoporous metal oxide films (< ~ 2 μm) compared to a liquid counterpart (> 10 μm) and a low open-circuit voltage (V_{oc}) value from many

recombination-inducing defects of incorporated QDs and their interfaces in the cell. Therefore, it is still necessary to search for more ideal photosensitizers to make efficient solid-state sensitized-type solar cells, which should have both defect-tolerance properties and high absorptivity over a broad range of the solar spectrum.

Over the last decade, bulk film-based organic/inorganic halide perovskites have displayed excellent optoelectronic properties [19,20] in many applicable structures such as photovoltaics [21,22], light-emitting devices [23], lasers [24], light-detectors [25], X-ray imaging [26], etc. In addition, nanoscale perovskites have also attracted much attention in a similar way as colloidal metal chalcogenide QDs [27]. Various nanocrystalline perovskites have been prepared in solution or inside nanoscale templates with easier and more versatile preparation routes such as precipitation and hot-injection [28,29]. Those nano-confined spheres, planes, wires, or others have shown a very high photoluminescence efficiency, approaching ~100 % in some cases [30-34]. Although each bulk- and nano-perovskite has been extensively explored in its own area, their relationships or correlations have rarely been studied. Recently, we have successfully shown that it is possible to prepare a representative perovskite of $MAPbI_3$ (MA: methylammonium) from well-separated nano-dots to well-connected bulk film through their intermediate forms by just controlling the concentration of lead iodide (PbI_2) used in the range from 0.10 to 1.2 M with the same preparative method for making $MAPbI_3$-based solar cells [35]. With another few trials [36-38], it looks clear that it is critical and sufficient to use a low concentration of lead halides, less than about 0.30 M, to prepare well-defined nanoscale $MAPbI_3$ photosensitizers over less than ~ 1 μm thick meso-TiO_2 film. To expand this method into a general way of preparing all kinds of nanoscale perovskites and also after being inspired by the recent development of efficient all-inorganic bulk perovskite-based solar cells [39-44], we have tried in this study to prepare all-inorganic nanoscale $CsPbI_xBr_{3-x}$

perovskite sensitizers on the surface of mesoporous TiO_2 films in a simple and general way with the controllability of its halide composition to modulate its absorption range. The as-prepared $CsPbI_xBr_{3-x}$ sensitizers were then tested instead of common molecular dyes in solid-state DSSCs and their roles were confirmed by the ideality factor and capacitance behavior of the perovskite-sensitized cells.

2. Experimental

2.1 Materials

Lead(II) iodide (PbI_2, 99.99%) and lead(II) bromide ($PbBr_2$) were purchased from TCI. Cesium iodide (CsI, 99.9%), cesium bromide (CsBr, 99.999%), *N,N*-dimethylformamide (DMF, anhydrous, 99.8%), methanol (anhydrous, 99.8%), spiro-OMeTAD (99%), chlorobenzene (anhydrous, 99.8%), 4-*tert*-butylpyridine (tBP, 96%), acetonitrile (anhydrous, 99.8%) and polyvinylpyrrolidone (PVP, M.W.: ~40,000) were purchased from Sigma-Aldrich. All the chemicals were used as received.

2.2 Device fabrication

Fluorine-doped tin oxide (FTO) glass electrodes were partially etched by a combination of zinc powder and HCl diluted solution on the target area. The substrate was cleaned with detergent, deionized (DI) water, and acetone, sequentially. A compact TiO_2 layer was applied on FTO by spray-pyrolysis done at 500 ^oC with a diluted solution of titanium(IV) diisopropoxide bis(acetylacetonate) in ethanol (1:25, v/v). Then, about 1 μm-thick mesoscopic TiO_2 layer was deposited over FTO/compact TiO_2 by spin-coating of diluted TiO_2 paste at a speed of 300 rpm for 5 s and continuously spun at 1000 rpm for 20 s, followed by annealing up to 500 ^oC gradually. The diluted TiO_2 paste was prepared by dissolving a 1.0 g of commercial

TiO_2 paste (Sharechem, SC-HT040) and a 0.02 g of PVP in 3 mL ethanol.

Nano-particulate $CsPbI_xBr_{3-x}$ perovskites were deposited on the meso-TiO_2 film by a two-step sequential process under a controlled humidity of 15~20% in a N_2-flowing box. A 100 μL of 0.30 M PbI_2 or $PbBr_2$ dissolved in DMF was spin-coated on the meso-TiO_2 film at 1000 rpm for 10 s and then 4000 rpm for 30 s. The as-deposited film was dried at 70 ºC for 10 min. After cooled down to room temperature, 500 μL of 0.03 M cesium iodide and/or bromide methanol solution was dropped on the PbI_2-adsorbed TiO_2 film during the spinning at 2000 rpm for 30 s. Then, the substrate was annealed at 250 ºC in a N_2-flowing box. For the details, a mixture of CsI and CsBr with different molar ratios such as 1:0 (sample 6), 7:3 (sample 5), 5:5 (sample 4), 3:7 (sample 3), and 0:1 (sample 2) was applied over TiO_2/PbI_2 film while keeping a total concentration of cesium halides at 0.03M. Sample 1 was prepared by applying 0.03 M CsBr over $TiO_2/PbBr_2$ film.

A 80 μL of spiro-OMeTAD solution was dropped on the perovskite-sensitized TiO_2 film and spin-coated at 500 rpm for 10 s first and then at 2500 rpm for 20 s. The spiro-OMeTAD solution was prepared by mixing its components in order to get a 80 mM of spiro-OMeTAD in chlorobenzene, a 64 mM of *t*BP, and 16 mM of Li-TFSI solution from the 1.0 M of stock solution which dissolved in acetonitrile. Finally, ~70 nm-thick gold (Au) layer was deposited on top area of the device by thermal evaporation for a counter electrode.

2.3 Characterization

The current-voltage characteristics (J-V curves) were measured in ambient atmosphere by using a potentiostat (IVIUM, CompactStat) and a solar simulator (Peccell, PEC-L01) under a simulated standard illuminating condition (100 mW cm^{-2}) after its intensity of the light source

was calibrated using a standard silicon photodiode from Peccell Technologies. The active area of solar cells measured was defined as 0.16 cm^2 by using a black shadow mask. The scan rate and voltage step in the J-V measurement were taken as 50 mV/s and 2 mV, respectively. The incident photon-to-current efficiency (IPCE) values from 380 to 800 nm were collected by using the integrated system supplied by the HS-Technologies based on a DC method without chopper and light bias. The stability of cell performances were checked by taking out the cells stored in a N_2 atmosphere and measuring J-V curves in ambient air over a time span of ~ 2 month.

Magnified film morphologies of $TiO_2/CsPbI_xBr_{3-x}$ were imaged by using a scanning electron microscope (SEM, SUPRA 40VP, Carl Zeiss) and a transmission electron microscopy (TEM, JEOL, JEM-ARM200F). As for determining the atomic ratio of iodide and bromide, EDXS were taken using an Apollo X (EDAX) over $TiO_2/CsPbI_xBr_{3-x}$ film. X-ray diffraction (XRD) measurements were done by X′pert Pro Powder (PANalytical) with Cu Kα radiation. For static photoluminescence measurements, the samples were irradiated by a cw beam of a 405 nm wavelength and the emission spectrum was measured by a spectrometer (SpectroPro HRS-300 from Princeton Instruments). In order to measure time-resolved photoluminescence, the time-correlated single photon counting (TCSPC) scheme was employed by using the Picoharp 300 (PicoQuant). In the scheme, the samples were photoexcited repetitively at 10 MHz with picosecond laser pulses of a 405 nm wavelength. The interval time between successive pulses was 100 ns which is long enough for the samples to relax via radiative or nonradiative recombination. The fitting analysis also yielded two decay time constants by assuming the time dependence as a linear combination of two exponential functions.

Impedance spectroscopy analysis was performed using an Autolab potentiostat using an

amplitude of the sinusoidal signal of 10 mV and scanning the impedance from 1 MHz to 100 mHz (down) and from 100 mHz to 1 MHz (up) in order to verify the reproducibility, see Supporting Information Figure S1. Impedances were measured by using different conditions: 1) changing the light intensity from the LED lamp using filters between 10 and 1000 W/m^2 and 2) changing the bias between 0.1 and 0.8 V keeping constant the light intensity at 100 W/m^2. Finally, all measures were fitted to equivalent circuit proposed [35] in order to compare the spectrums and determine the patterns.

2. Results and discussion

Figure 1 depicts how nano-particulate $CsPbI_xBr_{3-x}$ photosensitizers could be prepared directly on the surface of mesoscopic TiO_2 film with ~1 μm thickness by delivering their precursors in a sequential two-step way for making perovskite-sensitized solar cells. First, nanoscale aggregates of PbI_2 or $PbBr_2$ were deposited on the TiO_2 surface by spin-coating it at a relatively low concentration of 0.30 M compared to a typical high value (> 1.0 M) for well-known bulk perovskite films. Next, cesium halides with a different ratio of CsI and CsBr dissolved in methanol were dropped over the spinning PbI_2- or $PbBr_2$-adsorbed mesoscopic TiO_2 electrodes to induce the formation of nano-particulate $CsPbI_xBr_{3-x}$ perovskites all along the surface of the TiO_2 film. Finally, spiro-OMeTAD was infiltrated into the inner-space of the mesoporous electrode to make a hole-transporting channel followed by gold evaporation for a counter electrode. Then the photovoltaic performances of $CsPbI_xBr_{3-x}$-sensitized DSSC-type solid-state solar cells were tested under a standard simulated condition. When six cases of $CsPbI_xBr_{3-x}$ with different ratios of I and Br were tried, the color of electrodes became darkened as the amount of iodide increased but faded out easily in the two left-most ones with only or

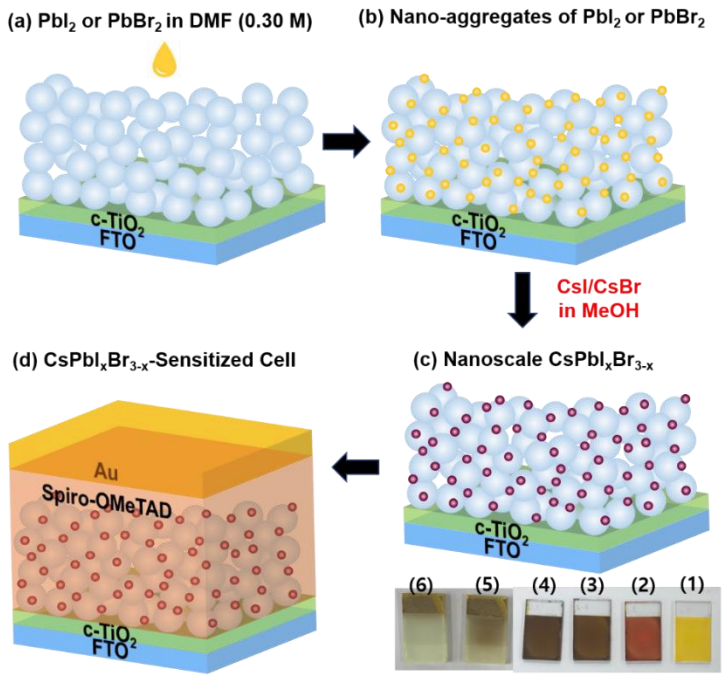

Figure 1. Scheme of step-wise preparation of nanoscale $CsPbI_xBr_{3-x}$ sensitizers on the surface of mesoscopic TiO_2 film for sensitized solar cells, (a) ~ (d). The picture of as-prepared electrodes is shown in the inset of (c), where (1) was from $TiO_2/PbBr_2$ reacted with CsBr while others were from TiO_2/PbI_2 reacted with a mixture of CsI and CsBr with a ratio of 0:1 (2), 3:7 (3), 5:5 (4), 7:3 (5), and 1:0 (6) by keeping a total concentration of halides same.

most iodide in halide compositions due to the reported destabilization of the as-formed black-phase in the air (inset picture in Figure 1c) [39,40]. From the experimental conditions used, samples (6) and (5) are expected to have a composition of $CsPbI_3$ and $CsPbI_xBr_{3-x}$ ($2 << x < 3$), respectively. It is well known from recent reports on bulk inorganic perovskites of $CsPbI_xBr_{3-x}$ that the desirable black-phases of $CsPbI_3$ and $CsPbI_2Br$ are not stable when exposed to the atmospheric air. Therefore, only the four right-most samples (1 ~ 4) were stable

and usable when prepared under a humidity condition of about 15~20% in the N_2-flowing box. To determine the ratio of iodide (I) and bromide (Br) after the preparation of $CsPbI_xBr_{3-x}$ by following the scheme described in Figures 1 (a) ~ (c), energy dispersive spectroscopy (EDS) elementary analysis was undertaken and their specific compositions were determined. Sample 1 was $CsPbBr_3$ because only Pb- and Cs-bromides were involved, while sample 2 was $CsPbI_{1.1}Br_{1.9}$, and samples 3 and 4 were proved to have a composition of $CsPbI_{1.9}Br_{1.1}$ and $CsPbI_{2.2}Br_{0.8}$, respectively. If the dropped CsBr was reacted only with the adsorbed PbI_2 in the expected stoichiometric ratio of 1:1 in preparing sample 2, the composition would have been $CsPbI_2Br$. But, in reality, a larger amount of CsBr was involved in the reaction with PbI_2 and replaced the present iodide partially, thus leading to more bromide-contained $CsPbI_{1.1}Br_{1.9}$. When the ratio of iodide and bromide in the solution used in second step increased to 3:7 for sample 3 from 0:1 for sample 2, the resulting perovskite was determined to be $CsPbI_{1.9}Br_{1.1}$ close to $CsPbI_2Br$. Therefore, in the two-step procedure at nanoscale deposition, the composition of cesium halides in the second step is more critical in determining the final composition of target perovskites. When the added amount of CsI was higher than that of CsBr in the second step (samples 5 and 6), the as-formed $CsPbI_xBr_{3-x}$ perovskites were unstable and soon de-colored in the air. Therefore, in this study, the four right-most samples (1~4) were tested further.

This proposed scheme of Figure 1 was checked by observing the surface status and morphologies of the meso-TiO_2 electrodes from SEM/TEM (Figure 2) and measuring the crystallinity of the as-formed $CsPbI_xBr_{3-x}$ perovskites from X-ray diffraction patterns (Figure 3) after applying the two steps shown in Figure 1. In contrast to the currently-dominating preparation routes for bulk perovskite films, low-concentrated lead (Pb) halides were spin-

coated, thus leading to scattered and separated deposition over ~ 1 μm-thick mesoporous TiO_2 film. Therefore, when the surface of TiO_2 film was imaged by SEM, it looked like a bare TiO_2 particle-connected porous film without perovskites even though the film displayed its characteristic color of $CsPbI_xBr_{3-x}$ depending on the halide ratio (Figure 2a and see the inset in Figure 1c). Taking a closer look at the TiO_2 surface by TEM (Figure 2b), dispersed hemi-dots with a size of few nanometers (3~6 nm) were seen to be deposited around the surface of TiO_2 particles (~50 nm). These TiO_2/nanoscale inorganic perovskites seemed to be almost the same apparently as those of successive ionic layer adsorption and reaction (SILAR)-deposited metal chalcogenide QDs in QD-sensitized solar cells [45-48] because they shared the same deposition processes based on a successive delivery of each precursor for direct contact and precipitation only on the surface of TiO_2.

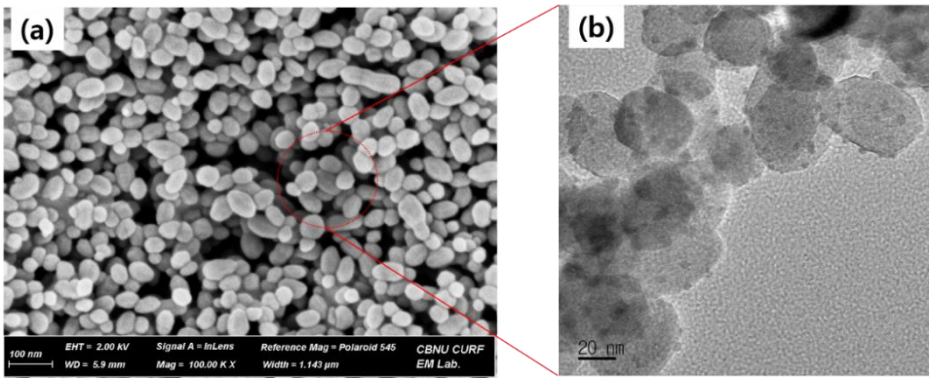

Figure 2. (a) SEM image of the top-surface and (b) TEM image of one part from the film in (a) after preparing $CsPbI_{2.2}Br_{0.8}$ on the surface of mesoporous TiO_2 film.

This *in-situ* preparation of nanoscale all-inorganic $CsPbI_xBr_{3-x}$ on TiO_2 has a few advantages of simple preparation and adjustment of composition along with a direct contact with ETM and

HTM without a group of long-chain insulating ligands such as oleic acid and amine which are generally surrounding perovskite colloidal nanocrystals [26,27]. This direct contact to charge-transporting materials without insulating ligands could be desirable for effective charge transfer to ETM and HTM after light absorption.

The characteristic crystallinities of as-prepared $CsPbI_xBr_{3-x}$ perovskites were checked by XRD measurements as shown in Figure 3. As the content of Br increased in the course of deposition of lead and cesium halides from sample 4 to sample 1, more Br-included $CsPbI_xBr_{3-x}$ was prepared as discussed above. The main peaks of $CsPbI_xBr_{3-x}$ perovskite in XRD gradually shifted to a larger angle due to the smaller lattice spacing of bromide (Br) included instead of iodide (I) as reported before [40,41]. These trends matched well with the formation of a homogeneous cubic perovskite structure of inorganic $CsPbI_xBr_{3-x}$. These XRD data also confirmed that the current two-step procedure is very effective for preparing all-inorganic nano-crystalline $CsPbI_xBr_{3-x}$ perovskites inside meso-TiO_2 film as a photosensitizer.

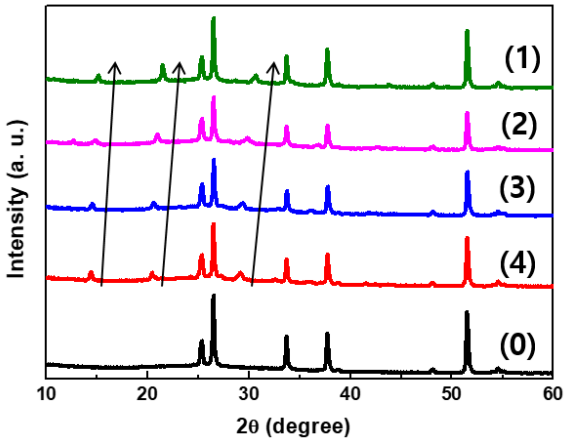

Figure 3. XRD patterns of FTO/TiO_2 film (0) and FTO/TiO_2/$CsPbI_xBr_{3-x}$ (1) ~ (4), where (1) was $CsPbBr_3$, (2) $CsPbI_{1.1}Br_{1.9}$, (3) $CsPbI_{1.9}Br_{1.1}$, and (4) $CsPbI_{2.2}Br_{0.8}$ (arrows are indicating

the shifts of main peaks for eye guidance).

Combined with the SEM/TEM and XRD data in Figures 2 and 3, the proposed scheme in Figure 1 looks appropriate and general for preparing nanoscale all-inorganic perovskites on the surface of mesoscopic metal oxide films as like in the preparation of SILAR-deposited QD sensitizers such as CdS [45], CdSe [46], PbS [47], etc [48]. In our previous reports, the representative perovskite of $MAPbI_3$ could also be grown at nanoscale by delivering its precursors, alternatively, where the Pb source was diverse as Pb^{2+}, PbI_2, or ionic liquid-complexed PbI_2 while the other source was the same as MAI and/or MABr [36-38]. By maintaining the concentration of the Pb source at less than about 0.30 M in the first step, well-separated nanoscale hemi dot-shaped $MAPbI_3Br_{3-x}$ perovskites could be prepared successfully on the surface of meso-TiO_2 film. From the current results, it looks common that the nanoscale formation of all-inorganic $CsPbI_3Br_{3-x}$ is also very similar to that of organic/inorganic $MAPbI_3Br_{3-x}$ and using low-concentrated lead halides is critical in preparing well-defined nano-perovskite photosensitizers over meso-TiO_2 film.

When these nanoscale $CsPbI_xBr_{3-x}$ perovskites were deposited on the surface of ZrO_2 in order to block the electron transfer after excitation and thus induce the radiative recombination, static and time-resolved photoluminescence (PL) could be measured clearly. Each steady-state PL was traced as one well-defined peak in all samples, indicating a homogeneous state of composition (Figure 4). As the Br content increased, a gradual blue-shift was observed and this agreed well with reported results of a similar composition in $CsPbI_xBr_{3-x}$ (Figure 4a). If time-resolved PL decay was traced, the more Br contents included, the faster decay was observed as summarized in the inset of Figure 4b.

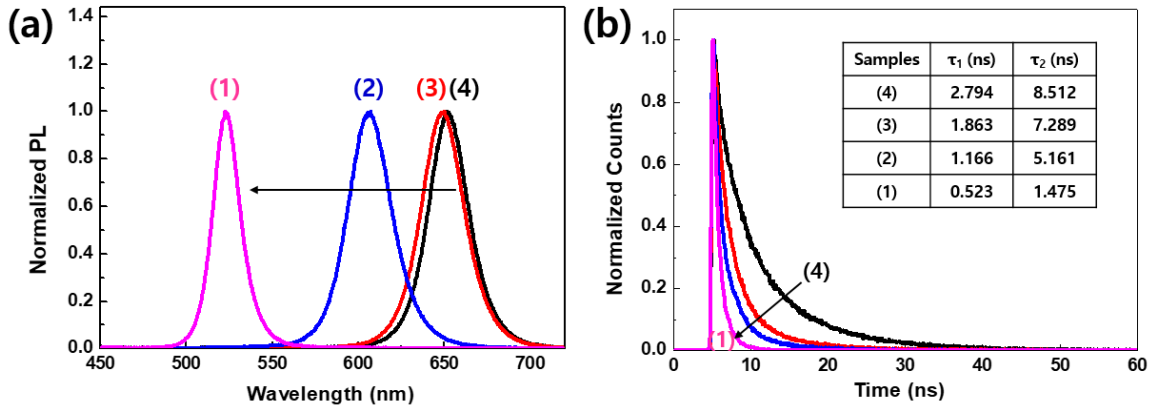

Figure 4. Static (a) and time-resolved (b) photoluminescences of glass/ZrO_2/$CsPbI_xBr_{3-x}$, where the content of Br increased towards the direction by arrow indicated [(1) $CsPbBr_3$, (2) $CsPbI_{1.1}Br_{1.9}$, (3) $CsPbI_{1.9}Br_{1.1}$, and (4) $CsPbI_{2.2}Br_{0.8}$].

These well-defined nanoscale hemi-dots of all-inorganic $CsPbI_xBr_{3-x}$ could be used as a photosensitizer in the cell structure of solid-state DSSCs by replacing conventional molecule-based dyes or metal chalcogenide QDs. After confirming the formation of nanoscale perovskites of $CsPbI_xBr_{3-x}$, their sensitized electrodes were tested first by combining spiro-OMeTAD as HTM and gold as a counter electrode. As shown in the IPCE curves of Figure 5(a), the onset point of current-flowing blue-shifted as the Br content increased from sample 4 to sample 1, which reflected well the colors of those sensitized electrodes. The initial overall power conversion efficiency (Figure 5b) was moderately good, over 1~3.5 % with a higher value from the ones containing more iodide in $CsPbI_xBr_{3-x}$ due to their wider absorption range and higher life-time as shown in Figure 4b. The best result was 3.78% (J_{sc}: 9.56 mA/cm^2, V_{oc}:

0.70 V, FF: 0.57) from a $CsPbI_{2.2}Br_{0.8}$-sensitized cell about four weeks after initial measurements. Though these PCEs obtained from nanoscale $CsPbI_xBr_{3-x}$ photosensitizers as a first attempt are not beyond the best ones reported from metal chalcogenide QDs after a long trial and error, it looks promising in terms of a few points such as 1) very facile preparation and modulation of absorption range of effective all inorganic perovskite photosensitizers attached directly on the surface of meso-TiO_2 film, 2) further optimizations of many parameters about the accumulated amount and density of deposited $CsPbI_xBr_{3-x}$ and interfacial modifications for reducing recombination processes, and 3) possible combinations with pre-existing sensitizers of molecular dyes and inorganic QDs for operative hybridization towards more efficient solid-state sensitized solar cells.

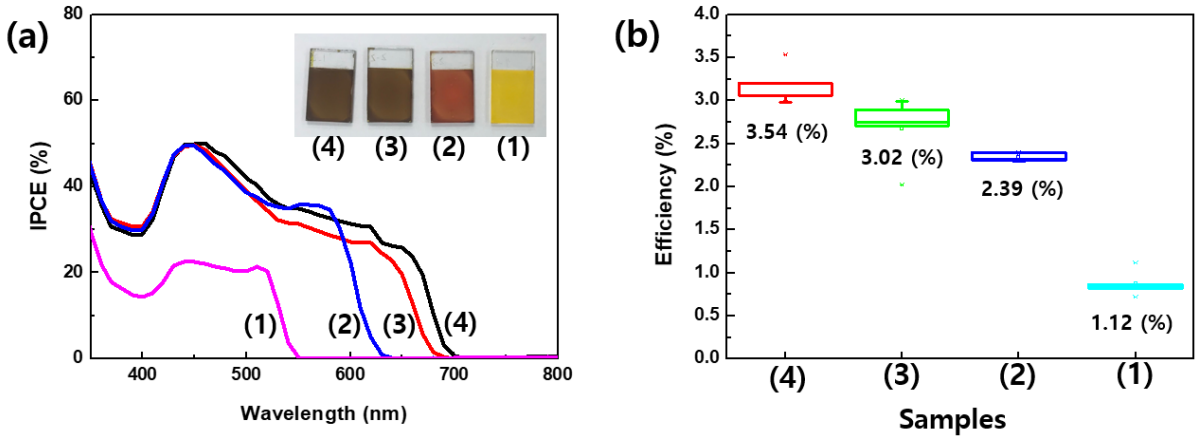

Figure 5 (a) IPCE and (b) statistical data set of initial power conversion efficiencies of $CsPbI_xBr_{3-x}$,-sensitized solar cells, where (1) was $CsPbBr_3$, (2) $CsPbI_{1.1}Br_{1.9}$, (3) $CsPbI_{1.9}Br_{1.1}$, and (4) $CsPbI_{2.2}Br_{0.8}$. The best initial power conversion efficiency is denoted below each statistical box.

When the well-known hysteresis in the current-voltage curves of bulk perovskite film-based solar cells was checked in the samples (2~4) in Figure 6a, no difference was seen depending on the direction of the voltage scan, showing a very stable trajectory in nano-sized $CsPbI_3Br_{3-x}$-sensitized cells. In contrast to the typical hysteresis behavior observed in bulk perovskite films, a few nanometer-sized all-inorganic $CsPbI_3Br_{3-x}$ perovskites seemed not to be affected by the migration of ions probably because the small size of perovskites strongly confined the halide ions and/or included bromide suppressed ion migration effectively [50]. The PCE records of samples (2, 3, and 4) were tracked for ~2 month to check the stability of $CsPbI_3Br_{3-x}$-sensitized cells. All the initial values increased by 10~30% before keeping a stable value and reached a maximum point after ~30 days (Figure 6b).

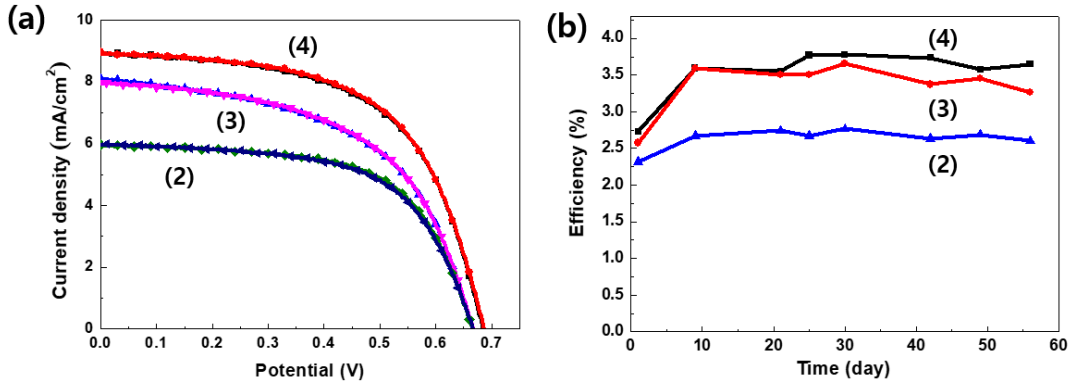

Figure 6. (a) Hysteresis of J-V curves (marker points are for forward while solid lines for backward scan) and (b) power stability check of $CsPbI_xBr_{3-x}$,-sensitized solar cells, where samples (2) ~ (4) are from those in Figure 5.

In order to obtain extra information about the devices with higher efficiencies ($CsPbI_{2.2}Br_{0.8}$), two samples were analyzed by impedance frequency response (IFR) changing the light

intensity and fixing the bias at the average V_{oc} recorded for one minute, see Figure S1 and Figure 7a. As both samples show similar impedance spectrum patterns and V_{oc} dependencies with light intensity, it is possible to validate the device reproducibly, reporting similar ideality factors (Figure 7b and Figure S1d) pointing to surface recombination process [49]. Well defined impedance behaviors were obtained allowing to estimate reliable capacitance spectrums (Figure 7c-d), which shows the main contribution of chemical capacitance at lower frequencies, related to mesoporous TiO_2 layer, being this a typical behavior of sensitize types cells [51]. In the case of ideality factor (n_{ID}), it was estimated from two independent ways as it was performed in previous work [38], one based on the relationship between V_{oc} and light intensities [49] (Figure S1c-d) and another estimated from the IFR considering bias and recombination resistances (R_{rec}) [35], (Figure 7b). Very good agreement for the calculation of n_{ID} from both procedures is observed. In addition, the capacitance was estimated from the IFR changing the bias (Figure 7c), confirming the capacitance behavior mentioned before. Finally, considering that ideality factor, impedance and capacitance spectrums, these look very similar among n_{ID}, and spectrums previously reported for DSSCs sensitized independently with both nanoscale $MAPbI_3$ and molecular dye (MK-2) [38], as should be expected for DSSCs. The chemical capacitance observed is related with the mesoporous TiO_2 layer independently of the sensitizer, and consequently sharing similar working principles, see Figure S2 in which a brief comparison is showed for a better visualization.

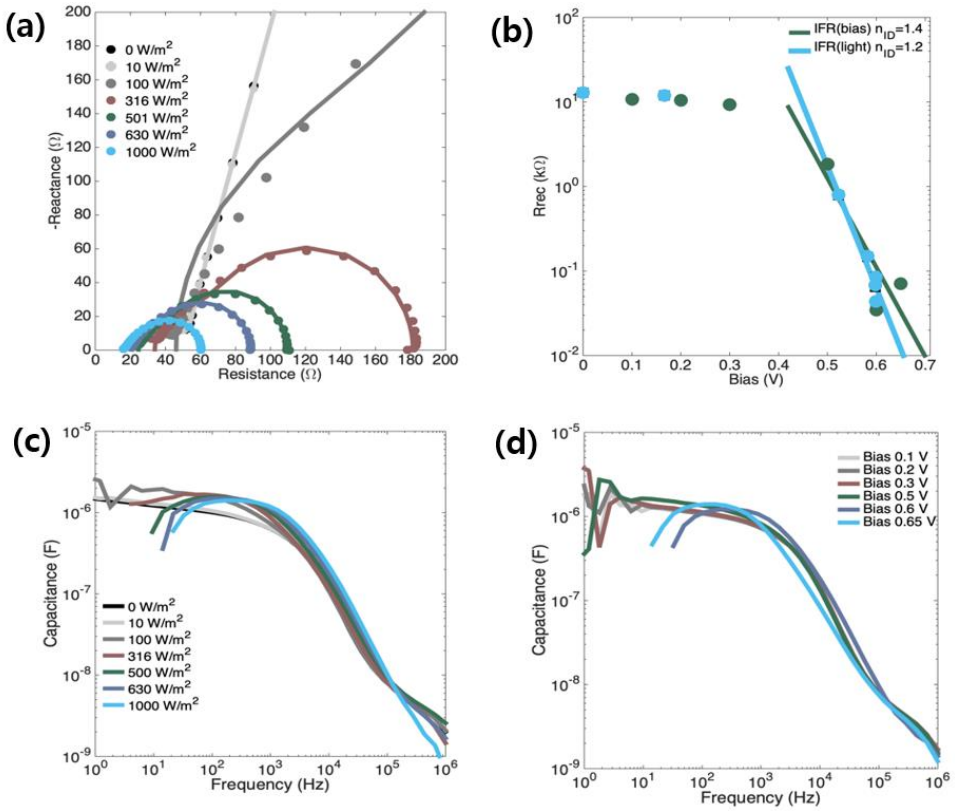

Figure 7. (a) Impedance Nyquist diagram as function of light intensities, corresponding the marker points to experimental data and solid lines to fits. (b) Estimated n_{ID} from the relationship between bias and R_{rec}. Green marker points are related to data obtained from the IFR changing bias, while blue marker points are from IFR changing light intensities (corresponding marker points to experimental data and solid lines to fit). Capacitance diagram estimated from the impedances as function of light intensities (c) and bias, fixing the light intensity at 100 W/m^2 (d).

3. Conclusions

In the pursuit of a new type of effective photosensitizer for solid-state DSSCs, we have successfully demonstrated in this study that a few nanometer-sized $CsPbI_xBr_{3-x}$ perovskites could be prepared directly by a simple two-step spin-coating of their precursors on the surface of ~1 μm-thick TiO_2 mesoscopic film for adoption in sensitized-type solar cells. The use of a low concentration of lead halides (0.30 M) has led to the well-scattered deposition of nanoscale aggregates and turned out to the target $CsPbI_xBr_{3-x}$ perovskites in the second step for the addition of cesium halides. Though it was possible to modulate the amount of bromide relative to iodide in $CsPbI_xBr_{3-x}$ and thus the absorption range by changing the ratio of halides involved in the two-step delivery of lead and cesium halides, pure $CsPbI_3$ or $CsPbI_xBr_{3-x}$ ($x >> \sim 2.2$) was found to be unstable when exposed to a laboratory atmosphere and another strategy should be considered for stabilizing those black-phase perovskites with a composition close to $CsPbI_3$. When stable nano-particulate $CsPbI_xBr_{3-x}$ perovskites were adopted in the position of molecular dye or metal chalcogenide QDs of solid-state DSSCs, they showed moderately good initial PCEs (ca. 1~3.5%) with a different range of sensitization depending on the amount of Br incorporated. Impedance frequency response analysis as function of light and bias confirmed that these nano-particulate $CsPbI_xBr_{3-x}$ works in the same way as molecular dye in DSSCs. Nanoscale $CsPbI_xBr_{3-x}$-sensitized mesoscopic TiO_2 film-based solar cells displayed no hysteresis in current-voltage curves and stable PCEs over ~2 month.

Along with recent advancement of bulk film-type $CsPbI_xBr_{3-x}$ in solar cell devices, the current nanoscale $CsPbI_xBr_{3-x}$ are expected to play an important role as an efficient photosensitizer for further developing sensitized-type solar cells. In addition, it will also be possible and interesting to combine inorganic metal chalcogenide QDs and all-inorganic

nanoscale $CsPbI_xBr_{3-x}$ perovskites in a sequential way on the same surface of meso-metal oxide films to make a more efficient hybrid sensitizer unit composed of QD/perovskite at nanoscale.

Acknowledgement

H. J. Lee acknowledges the financial support by the National Research Foundation (NRF-2019R1A1A2057772) and T. Shin thanks the support from no. 2012R1A1A1015528 of NRF. I. Mora-Seró acknowledges Generalitat Valenciana via Prometeo Grant Q-Devices (Prometeo/2018/098). Esteban Velilla acknowledge the financial support provided by Colombia′s Administrative Department of Science Technology and Innovation (COLCIENCIAS), contract No. FP44842-124-2017 (national doctoral scholarship No. 727-2015), and by the Colombia Scientific Program within the framework of the call Ecosistema Científico (Contract No. FP44842- 218-2018).

Supporting Information Available

Data of ideality factor and capacitance from impedance measurements and their comparisons with MK-2 dye and nanoscale $MAPbI_3$ are given. This information is available free of charge.

References

[1] Z. Pan, H. Rao, I. Mora-Seró, J. Bisquert, X. Zhong, Quantum Dot-Sensitized Solar Cells, Chem. Soc. Rev. 47 (2018) 7659-7702.

[2] I. Mora-Seró, Current Challenges in the Development of Quantum Dot Sensitized Solar Cells, Adv. Energy Mater. 10 (2020) 2001774.

[3] S. Jiao, J. Du, Z. Du, D. Long, W. Jiang, Z. Pan, Y. Li, X. Zhong, Nitrogen-Doped Mesoporous Carbons as Counter Electrodes in Quantum Dot Sensitized Solar Cells with a Conversion Efficiency Exceeding 12%, *J. Phys. Chem. Lett.*, 8(2017) 559 -564.

[4] Z. Pan, L. Yue, H. Rao, J. Zhang, X. Zhong, Z. Zhu, A. K.-Y. Jen, Boosting the Performance of Environmentally Friendly Quantum Dot-Sensitized Solar Cells over 13% Efficiency by Dual Sensitizers with Cascade Energy Structure, Adv. Mater. 31(2019) 1903696.

[5] B. O'Regan, M. Grätzel, A Low-Cost, High-Efficiency Solar Cell Based on Dye-Sensitized Colloidal TiO_2 Films, Nature 353(1991) 737-740.

[6] A. Hagfeldt, G. Boschloo, L. C. Sun, L. Kloo, H. Pettersson, Dye-Sensitized Solar Cells, Chem. Rev. 110(2010) 6595-6663.

[7] S. Mathew, A. Yella, P. Gao, R. Humphry-Baker, B. F. E. Curchod, N. Ashari-Astani, I. Tavernelli, U. Rothlisberger, Md. K. Nazeeruddin, M. Grätzel, Dye-sensitized solar cells with 13% efficiency achieved through the molecular engineering of porphyrin sensitizers, Nature Chemistry 6(2014) 242-247.

[8] Z. Pan, K. Zhao, J. Wang, H. Zhang, Y. Feng, X. Zhong, Near Infrared Absorption of $CdSe_xTe_{1-x}$ Alloyed Quantum Dot Sensitized Solar Cells with More than 6% Efficiency and High Stability, ACS Nano 7(2013) 5215-5222.

[9] J. Du, Z. Du, J.-S. Hu, Z. Pan, Q. Shen, J. Sun, D. Long, H. Dong, L. Sun, X. Zhong, L.-J. Wan, Zn–Cu–In–Se Quantum Dot Solar Cells with a Certified Power Conversion Efficiency

of 11.6%, J. Am. Chem. Soc. 138(2016) 4201-4209.

[10] W. Wang, H. Rao, W. Fang, H. Zhang, M. Zhou, Z. Pan, X. Zhong, Enhancing Loading Amount and Performance of Quantum-Dot-Sensitized Solar Cells Based on Direct Adsorption of Quantum Dots from Bicomponent Solvents, J. Phys. Chem. Lett. 10(2019) 229-237.

[11] W. Wang, W. Feng, J. Du, W. Xue, L. Zhang, L. Zhao, Y. Li, X. Zhong, Cosensitized Quantum Dot Solar Cells with Conversion Efficiency over 12%, Adv. Mater. 30(2018) 1705746.

[12] S. Ruhle, S. Yahav, S. Greenwald, A. Zaban, Importance of Recombination at the TCO/Electrolyte Interface for High Efficiency Quantum Dot Sensitized Solar Cells, J. Phys. Chem. C 116**(**2012)17473-17478.

[13] K. Zhao, Z. Pan, X. Zhong, Charge Recombination Control for High Efficiency Quantum Dot Sensitized Solar Cells, J. Phys. Chem. Lett. 7(2016) 406-417.

[14] R. Plass, S. Pelet, J. Krueger, M. Grätzel, U. Bach, Quantum Dot Sensitization of Organic−Inorganic Hybrid Solar Cells, J. Phys. Chem. B 106(2002) 7578-7580.

[15] H. J. Lee, H. C. Leventis, S.-J. Moon, P. Chen, S. Ito, S. A. Haque, T. Torres, F. Nuesch, T. Geiger, S. M. Zakeeruddin, M. Gratzel, M. K. Nazeeruddin, PbS and CdS Quantum Dot-Sensitized Solid-State Solar Cells: "Old Concepts, New Results", Adv. Funct. Mater. 19(2009) 2735-2742.

[16] Y. C. Choi, D. U. Lee, J. H. Noh, E. K. Kim, S. I. Seok, Highly Improved Sb_2S_3 Sensitized-Inorganic-Organic Heterojunction Solar Cells and Quantification of Traps by Deep-Level Transient Spectroscopy, Adv. Funct. Mater. 24(2014) 3587-3592.

[17] K. C. Godel, Y. C. Choi, B. Roose, A. Sadhanala, H. J. Snaith, S. I. Seok, U. Steiner, S. K. Pathak, Efficient room temperature aqueous Sb_2S_3 synthesis for inorganic-organic sensitized solar cells with 5.1% efficiencies, Chem. Commun. 51(2015) 8640-8643.

[18] J. P. Park, J. H. Heo, S. H. Im, S.-W. Kim, Highly efficient solid-state mesoscopic PbS with embedded CuS quantum dot-sensitized solar cells, J. Mater. Chem. A 4(2016) 785-790.

[19] Y. Zhao, K. Zhu, Organic–inorganic hybrid lead halide perovskites for optoelectronic and electronic applications, Chem. Soc. Rev. 45(2016) 655-689.

[20] H. Chen, H. Wang, J. Wu, F. Wang, T. Zhang, Y. Wang, D. Liu, S. Li, R. V. Penty, lan H. White, Flexible optoelectronic devices based on metal halide perovskites, Nano Res. 13(2020) 1997-2018.

[21] J. Y. Kim, J.-W. Lee, H. S. Jung, H. Shin, N.-G. Park, High-Efficiency Perovskite Solar Cells, Chem. Rev. 120(2020) 7867-7918.

[22] A. K. Jena, A. Kulkarni, T. Miyasaka, Halide Perovskite Photovoltaics: Background, Status, and Future Prospects, Chem. Rev. 119(2019) 3036-3103.

[23] Q. V. Le, H. W. Jang, S. Y. Kim, Recent Advances toward High-Efficiency Halide Perovskite Light-Emitting Diodes: Review and Perspective, Small Methods 2(2018) 1700419.

[24] K. Wang, S. Wang, S. Xiao, Q. Song, Recent Advances in Perovskite Micro- and Nanolasers, Adv. Opt. Mater. 6(2018) 1800278.

[25] M. Ahmadi, T. Wu, B. Hu, A Review on Organic–Inorganic Halide Perovskite Photodetectors: Device Engineering and Fundamental Physics, Adv. Mater. 29(2017) 1605242.

[26] M. Sytnyk, S. Deumel, S. F. Tedde, G. J. Matt, W. Heiss, A perspective on the bright future of metal halide perovskites for X-ray detection, Appl. Phys. Lett. 115(2019) 190501.

[27] J. Shamsi, A. S. Urban, M. Imran, L. De Trizio, L. Manna, Metal Halide Perovskite Nanocrystals: Synthesis, Post-Synthesis Modifications, and Their Optical Properties, Chem. Rev. 119(2019) 3296-3348.

[28] S. A. Kulkarni, S. G. Mhaisalkar, N. Mathews, P. P. Boix, Perovskite Nanoparticles:

Synthesis, Properties, and Novel Applications in Photovoltaics and LEDs, Small Methods 3(2019) 1800231.

[29] L. Protesescu, S. Yakunin, M. I. Bodnarchuk, F. Krieg, R. Caputo, C. H. Hendon, R. X. Yang, A. Walsh, M. V. Kovalenko, Nanocrystals of Cesium Lead Halide Perovskites (CsPbX3, X = Cl, Br, and I): Novel Optoelectronic Materials Showing Bright Emission with Wide Color Gamut, Nano Lett. 15(2015) 3692-3696.

[30] L. Polavarapu, B. Nickel, J. Feldmann, A. S. Urban, Advances in Quantum-Confined Perovskite Nanocrystals for Optoelectronics, Adv. Energy Mater. 7(2017) 1700267.

[31] V. Malgras, S. Tominaka, J. W. Ryan, J. Henzie, T. Takei, K. Ohara, Y. Yamauchi, Observation of Quantum Confinement in Monodisperse Methylammonium Lead Halide Perovskite Nanocrystals Embedded in Mesoporous Silica, J. Am. Chem. Soc. 138(2016) 13874.

[32] Y. Bekenstein, B. A. Koscher, S. W. Eaton, P. Yang, A. P. Alivisatos, Highly Luminescent Colloidal Nanoplates of Perovskite Cesium Lead Halide and Their Oriented Assemblies, J. Am. Chem. Soc. 137(2015) 16008.

[33] S. Demchyshyn, J. M. Roemer, H. Groiss, H. Heilbrunner, C. Ulbricht, D. Apaydin, A. Bohm, U. Rutt, F. Bertram, G. Hesser, M. C. Scharber, N. S. Sariciftci, B. Nickel, S. Bauer, E. D. Glowacki, M. Kaltenbrunner, Confining metal-halide perovskites in nanoporous thin films, Sci. Adv. 3(2017) e1700738.

[34] F. Liu, Y. Zhang, C. Ding, S. Kobayashi, T. Izuishi, N. Nakazawa, T. Toyoda, T. Ohta, S. Hayase, T. Minemoto, K. Yoshino, S. Dai, Q. Shen, Highly Luminescent Phase-Stable $CsPbI_3$ Perovskite Quantum Dots Achieving Near 100% Absolute Photoluminescence Quantum Yield, ACS Nano 11(2017) 10373-10383.

[35] S.-M. Yoo, S. J. Yoon, J. A. Anta, H. J. Lee, P. P. Boix, I. Mora-Seró, An Equivalent Circuit for Perovskite Solar Cell Bridging Sensitized to Thin Film Architectures, Joule 3(2019) 2535-

2549.

[36] H. J. Lee, K. T. Cho, S. Paek, Y. Lee, A. J. Huckaba, V. I. E. Queloz, I. Zimmermann, G. Grancini, E. Oveisi, S.-M. Yoo, S.-Y. Lee, T. Shin, M. Kim, M. K. Nazeeruddin, A Facile Preparative Route of Nanoscale Perovskites over Mesoporous Metal Oxide Films and Their Applications to Photosensitizers and Light-Emitters, Adv. Funct. Mater. 28(2018) 1803801.

[37] M. Kim, S.-Y. Lee, S.-M. Yoo, S. Paek, Y. Lee, K. T. Cho, I. Zimmermann, H.-Y. Kim, B.-S. Kim, M.-K. Song, T. Shin, K. Kim, A. J. Huckaba, M. K. Nazeeruddin, H. J. Lee, Effective Preparation of Nanoscale $CH_3NH_3PbI_3$ Perovskite Photosensitizers for Mesoporous TiO_2-Based Solar Cells by Successive Precursor Layer Adsorption and Reaction (SPLAR) Process, Energy Technol. 8(2020) 1901186.

[38] S.-M. Yoo, S.-Y. Lee, E. V. Hernandez, M. Kim, G. Kim, T. Shin, M. K. Nazeeruddin, I. Mora-Seró, H. J. Lee, Nanoscale Perovskite-Sensitized Solar Cell Revisited: Dye-Cell or Perovskite-Cell? ChemSusChem 13(2020) 2571-2576.

[39] G. E. Eperon, G. M. Paterno, R. J. Sutton, A. Zampetti, A. A. Haghighirad, F. Cacialli, H. J. Snaith, Inorganic caesium lead iodide perovskite solar cells, J. Mater. Chem. A, 3(2015) 19688-19695.

[40] R. J. Sutton, G. E. Eperon, L. Miranda, E. S. Parrott, B. A. Kamino, J. B. Patel, M. T. Hörantner, M. B. Johnston, A. A. Haghighirad, D. T. Moore, H. J. Snaith, Bandgap-Tunable Cesium Lead Halide Perovskites with High Thermal Stability for Efficient Solar Cells, Adv. Energy Mater. 6(2016) 1502458.

[41] N. A. N. Ouedraogo, Y. Chen, Y. Y. Xiao, Q. Meng, C. B. Han, H. Yan, Y. Zhang, Stability of all-inorganic perovskite solar cells, Nano Energy 67 (2020) 104249.

[42] M. B. Faheem, B. Khan, C. Feng, M. U. Farooq, F. Raziq, Y. Xiao, Y. Li, All-Inorganic Perovskite Solar Cells: Energetics, Key Challenges, and Strategies toward Commercialization,

ACS Energy Lett. 5(2020) 290-320.

[43] H. Chen, S. Xiang, W. Li, H. Liu, L. Zhu, S. Yang, Inorganic Perovskite Solar Cells: A Rapidly Growing Field, Sol. RRL 2(2018) 1700188.

[44] Q. Tai, K.-C. Tang, F. Yan, Recent progress of inorganic perovskite solar cells, Energy Environ. Sci., 12(2019) 2375-2405.

[45] Kim, M.; Ochirbat, A.; Lee, H. J. CuS/CdS Quantum Dot Composite Sensitizer and Its Applications to Various TiO_2 Mesoporous Film-Based Solar Cell Devices, Langmuir 31(2015) 7609-7615.

[46] Lee, H.; Wang, M. K.; Chen, P.; Gamelin, D. R.; Zakeeruddin, S. M.; Gratzel, M.; Nazeeruddin, M. K. Efficient CdSe Quantum Dot-Sensitized Solar Cells Prepared by an Improved Successive Ionic Layer Adsorption and Reaction Process, Nano Lett. 9(2009) 4221-4227.

[47] Tian, J.; Shen, T.; Liu, X.; Fei, C.; Lv, L.; Cao, G. Enhanced Performance of PbS Quantum-Dot-Sensitized Solar Cells via Optimizing Precursor Solution and Electrolytes, Sci. Rep. 6(2016) 23094.

[48] Pathan, H. M.; Lokhande, C. D. Deposition of Metal Chalcogenide Thin Films by Successive Ionic Layer Adsorption and Reaction (SILAR) Method, Bull. Mater. Sci. 27(2004) 85-111.

[49] Tress, W.; Yavari, M.; Domanski, K.; Yadav, P.; Niesen, B.; Baena, J. P. C.; Hagfeldt, A.; Graetzel, M. Interpretation and Evolution of Open-Circuit Voltage, Recombination, Ideality Factor and Subgap Defect States during Reversible Light-Soaking and Irreversible Degradation of Perovskite Solar Cells, Energy Environ. Sci. 11(2018) 151-165.

[50] Zhang, T.; Chen, H.; Bai, Y.; Xiao, S.; Zhu, L.; Hu, C.; Xue, Q.; Yang, S. Understanding the Relationship between Ion Migration and the Anomalous Hysteresis in High-Efficiency

Perovskite Solar Cells: A Fresh Perspective from Halide Substitution, Nano Energy 26(2016) 620-630.

[51] Fabregat-Santiago, F.; Garcia-Belmonte, G.; Mora-Seró, I.; Bisquert, J. Characterization of Nanostructured Hybrid and Organic solar cells by Impedance Spectroscopy, Phys. Chem. Chem. Phys. 13(2011) 9083-9118.

Supporting Information

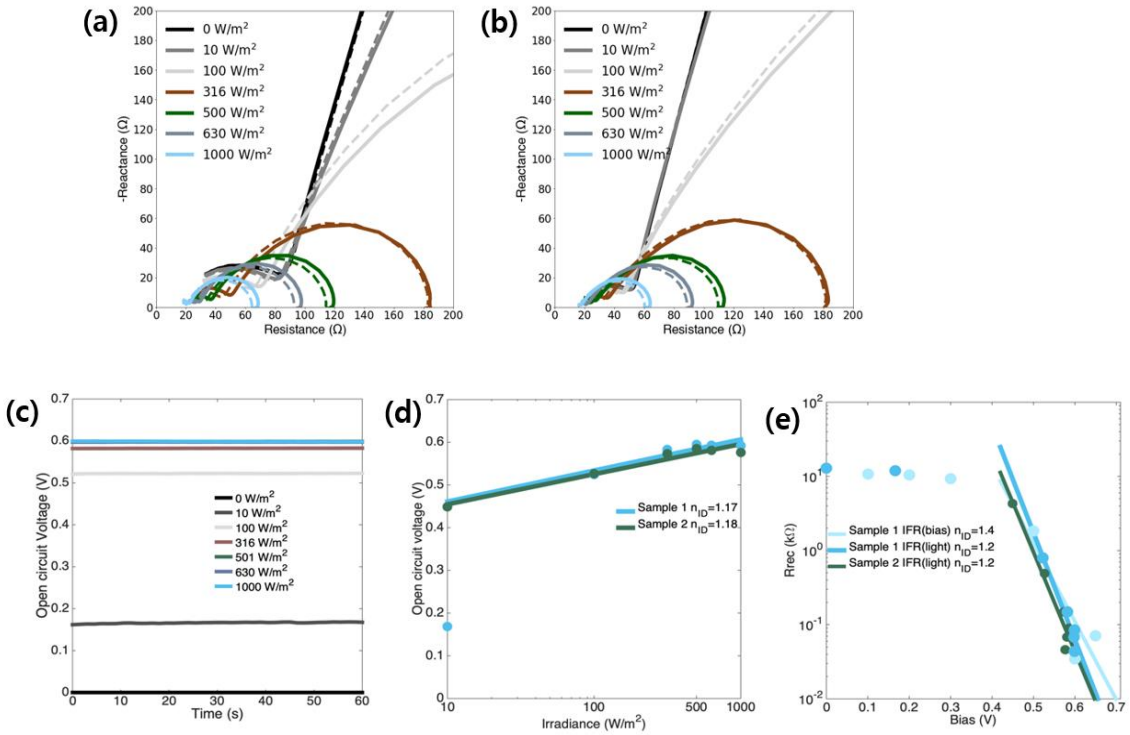

Figure S1. **(a-b)** Impedance Nyquist diagrams of two samples analyzed by changing the light intensity. Solid lines are related to impedance scanned data from high to low frequencies (down), while marker points from low to high frequency (up). Corresponding (a) to sample 1 and (b) to sample 2. **(c)** V_{oc} recorded for 1 minute after the changes on the light intensity for sample 1, in order to determine the average value to be considered as bias in the IFR. **(d)** Estimated n_{ID} of both samples from the relationship between light intensity and V_{oc}, considering the V_{oc} as the average value during one minute before to perform the IFR at each light intensity, blue color for sample 1 and green color for sample 2. **(e)** n_{ID} was also estimated for sample 1 changing the bias in the IFR. Corresponding marker points to experimental data and solid lines to fit.

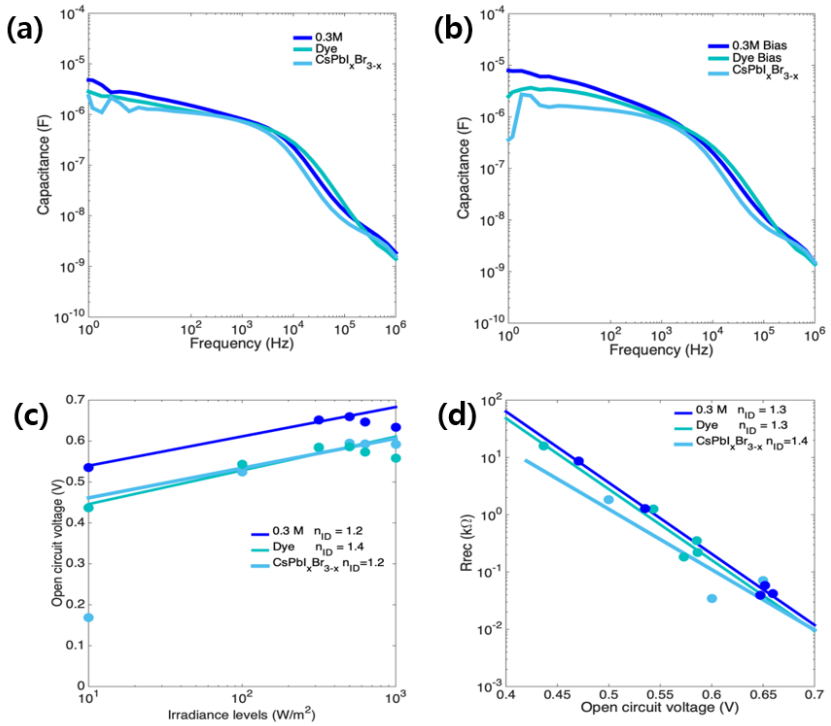

Figure S2. Comparing capacitance at **(a)** 0.2 and **(b)** 0.5 V of bias and fixing the light intensity at 100 W/m^2, among dye (MK-2)-, nanoscale $MAPbI_3$- and nanoscale $CsPbI_{2.2}Br_{0.8}$-sensitized cells. **(c)** Comparing ideality factor estimated from V_{oc} and light intensities among nanoscale $MAPbI_3$-, dye (MK-2)- and nanoscale $CsPbI_{2.2}Br_{0.8}$-sensitized cells. **(d)** Comparing ideality factor from impedance frequency response at different bias fixing the light intensity at 100 W/m^2 among nanoscale $MAPbI_3$-, dye (MK-2)- and nanoscale $CsPbI_{2.2}Br_{0.8}$-sensitized cells. (Data from nanoscale $MAPbI_3$- and dye (MK-2)-sensitized cells were adopted from our previous report [1] for comparison with nanoscale $CsPbI_{2.2}Br_{0.8}$-sensitized cell from current study)

[1] S.-M. Yoo, S.-Y. Lee, E. V. Hernandez, M. Kim, G. Kim, T. Shin, M. K. Nazeeruddin, I. Mora-Seró, H. J. Lee, Nanoscale Perovskite-Sensitized Solar Cell Revisited: Dye-Cell or Perovskite-Cell? ChemSusChem 13(2020) 2571-2576.